



A Journal of the Gesellschaft Deutscher Chemiker

# Angewandte Chemie

GDCh

International Edition

www.angewandte.org

## Accepted Article

**Title:** In situ Generation and Stabilization of Accessible Cu/Cu<sub>2</sub>O Heterojunctions inside Organic Frameworks for Highly Efficient Catalysis

**Authors:** Chuan-De Wu, Kai Chen, and Jia-Long Ling

This manuscript has been accepted after peer review and appears as an Accepted Article online prior to editing, proofing, and formal publication of the final Version of Record (VoR). This work is currently citable by using the Digital Object Identifier (DOI) given below. The VoR will be published online in Early View as soon as possible and may be different to this Accepted Article as a result of editing. Readers should obtain the VoR from the journal website shown below when it is published to ensure accuracy of information. The authors are responsible for the content of this Accepted Article.

**To be cited as:** *Angew. Chem. Int. Ed.* 10.1002/anie.201913811  
*Angew. Chem.* 10.1002/ange.201913811

**Link to VoR:** <http://dx.doi.org/10.1002/anie.201913811>  
<http://dx.doi.org/10.1002/ange.201913811>

# In situ Generation and Stabilization of Accessible Cu/Cu<sub>2</sub>O Heterojunctions inside Organic Frameworks for Highly Efficient Catalysis

Kai Chen<sup>[a]</sup>, Jia-Long Ling<sup>[a]</sup> and Chuan-De Wu<sup>\*[a]</sup>

**Abstract:** Heterostructural metal/metal oxides are the very promising substituents of noble-metal catalysts; however, generation and further stabilization of accessible metal/metal oxide heterojunctions are very difficult. Herein, a strategy to in situ encapsulate and stabilize Cu/Cu<sub>2</sub>O nanojunctions in porous organic frameworks is developed by tuning the acrylate contents in copper-based metal-organic frameworks (Cu-MOFs) and the pyrolytic conditions. The acrylate groups play important roles on improving the polymerization degree of organic frameworks, and generating and stabilizing highly dispersed and accessible Cu/Cu<sub>2</sub>O heteronanojunctions. As a result, pyrolysis of the MOF ZJU-199, consisting of three acrylates per ligand, generates abundant heterostructural Cu/Cu<sub>2</sub>O discrete domains inside porous organic matrices at 350 °C, demonstrating excellent catalytic properties in liquid-phase hydrogenation of furfural into furfuryl alcohol, which are much superior to the non-noble metal-based catalysts in the literature. This work provides a promising pathway for developing highly efficient non-noble metal catalysts in practical applications.

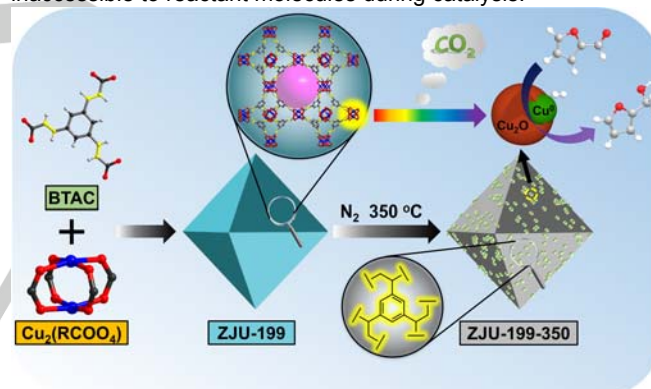
## Introduction

Noble metal catalysts (e.g. Pd, Pt, Au and Rh) are highly active in numerous chemical processes, attributed to their unique electron and orbital properties.<sup>1</sup> However, the high-cost and scarcity of noble metals heavily hindered their practical applications. A tremendous effort has been paid on developing the alternatives with earth-abundant metal sources, including metal/metal oxide nanoparticles (MNPs); however, their catalytic properties remain much inferior to those of noble catalysts.<sup>2</sup> In accordance with the unique electron donating and accepting properties of noble metals, the most promising alternative catalysts based on earth-abundant metals should consist of heterojunctions, in which one could act as the redox-active center while the other one should perform as the Lewis acid or base site, which would synergistically work to mimic the electron and orbital properties of noble metals.<sup>3</sup>

Among numerous earth-abundant metal/metal oxides, Cu-based nanomaterials are highly attractive, because the copper element could form valence-mixed heterostructures, such as Cu/Cu<sub>2</sub>O, Cu<sub>2</sub>O/CuO and Cu/Cu<sub>2</sub>O/CuO.<sup>4</sup> In contrast to the isolated single phase of Cu or CuO<sub>x</sub>, the Cu/CuO<sub>x</sub> heterostructures could re-localize the electron densities of different redox-active sites on the interfaces, resulting in

decreased transition energy barriers during catalysis.<sup>5</sup> However, the exposed active metallic copper is easily oxidized to form CuO<sub>x</sub> coating layers, leading to the heterostructural Cu/CuO<sub>x</sub> interfaces inaccessible, and thus to heavily deteriorate the catalytic properties.<sup>6</sup>

Metal-organic frameworks (MOFs) are a class of porous crystalline materials, constructed from the coordination bond connections between multidentate organic linkers and metal ions/clusters, which have been extensively used to fabricate porous MNPs@carbon composites under high temperature pyrolytic conditions.<sup>7</sup> MNPs@carbon composites exhibited high catalytic efficiency in numerous reactions, attributed to the in situ formed graphitic carbons that provide good electron mobility to promote charge separation/transfer. However, extreme high annealing temperature often resulted in severe collapse of the pristine skeletons of MOFs and subsequent aggregation of in situ formed MNPs, leading to the formation of thermally stable homogeneous phases or the heterojunction interfaces inaccessible to reactant molecules during catalysis.<sup>8</sup>



**Scheme 1.** Schematic illustration of the preparation of porous organic frameworks, consisting of in situ generated heterostructural Cu/Cu<sub>2</sub>O nanoparticles, for liquid phase hydrogenation of FAL into FOL.

It has been demonstrated that cinnamic acid could be decarboxylated to produce styrene and further polymerized at 200–270 °C in the presence of CuSO<sub>4</sub> catalyst.<sup>9</sup> Therefore, the Cu-MOFs, consisting of multiple acrylate moieties in organic linkers, should be an ideal class of porous templates for the fabrication of porous organic frameworks under suitable pyrolytic conditions.<sup>10</sup> The polystyrene networks might perform as robust physical barriers to prevent the migration of in situ formed copper nanospecies during pyrolysis, resulting in abundant accessible Cu/CuO<sub>x</sub> nanojunctions inside porous organic matrices. As shown in **Scheme 1**, the sizes, compositions and heterostructures of in situ generated Cu/CuO<sub>x</sub> nanoparticles inside porous organic frameworks are indeed systematically tunable by adjusting the constituents and functionalities of organic linkers in Cu-MOFs and controlling the annealing

[a] K. Chen, J.-L. Ling and Prof. Dr. C.-D. Wu  
State Key Laboratory of Silicon Materials  
Department of Chemistry  
Zhejiang University  
Hangzhou 310027, P. R. China  
E-mail: cdwu@zju.edu.cn

Supporting information for this article is given via a link at the end of the document.

conditions, which realized high catalytic efficiency, selectivity and stability in liquid phase hydrogenation of furfural (FAL) into furfuryl alcohol (FOL).

## Results and Discussion

The Cu-MOF ZJU-199 (ZJU = Zhejiang University) is built from  $[\text{Cu}_2(\text{COO})_4]$  paddle-wheel secondary building units (SBUs) and benzene-1,3,5-tri- $\beta$ -acrylate (BTAC) linkers, sharing the same tbo topology and coordination modes with the Cu-MOF HKUST-1.<sup>11</sup> There are three acrylate moieties per ligand, indicating that ZJU-199 should be an ideal precursor for the preparation of porous organic frameworks consisting of in situ generated Cu/CuO<sub>x</sub> nanojunctions (Figure S1 and Scheme S1). We first monitored the thermal behaviors of ZJU-199 by TG-MS measurement under inert N<sub>2</sub> atmosphere (Figure 1a). The weight loss before 150 °C should be assigned to the release of encapsulated solvent and coordinated water molecules. Upon raising the temperature, a weight loss of 22.1 wt% was observed in the range of 250–400 °C. Based on the overlap of DTG curve and corresponding CO<sub>2</sub> mass plot, the weight loss should be originated from decarboxylation of organic linkers. The weight loss is smaller than the content of exact carboxylate groups (28.6 wt%) in ZJU-199, indicating that there should occur other decomposition pathways besides of decarboxylation, such as trapping part of the carboxylate moieties in the form of carbonyl or ester moieties in the residues, because there is no obvious emission of CO<sub>2</sub> gas afterwards (Scheme S2).<sup>12</sup> Another weight loss from 400 to 500 °C should be attributed to further dehydrogenation and condensation of organic moieties. When raising the temperature to 800 °C, the retained residue is of 51.0 wt%, closing to the sum of calculated masses for copper element (20.8 wt%) and decarboxylated moieties (33.1 wt%) in ZJU-199, indicating no obvious organic weight loss occurred during the carbonization process. In contrast, a remarkable weight loss (41.0 wt%) is observed in the temperature range from 250 to 400 °C for HKUST-1, which is greatly higher than the calculated value (31.4 wt%) for the carboxylate groups (Figure 1b). When the temperature was raised to 800 °C, only 26.2 wt% of residual mass was obtained for HKUST-1, which is slightly higher than the copper content (22.8 wt%). The above results clearly demonstrated that the presence of acrylate moieties in organic ligands could markedly prevent the evaporation of organic moieties under pyrolytic conditions, which might fabricate physical barriers to inhibit the agglomeration of in situ formed MNPs.

According to the TG results, ZJU-199 was pyrolyzed at different temperatures for 2 h under N<sub>2</sub> atmosphere to prepare Cu/CuO<sub>x</sub>@organic framework composites, denoted as ZJU-199-T (T = temperature). FT-IR spectra show that there is a broad decarboxylation process for ZJU-199 from 250 to 350 °C (Figure 2a). The characteristic signals of aromatic moieties in decarboxylated ZJU-199-350 appear at 1595 and 1440 cm<sup>-1</sup>.

There also appears an obvious C=O vibration band at 1670 cm<sup>-1</sup>, which is in line with the TG results, indicating that there are multiple cross-linking pathways for the organic residues under pyrolytic conditions. The characteristic peak of exocyclic C=C vibration at 980 cm<sup>-1</sup> gradually decreases upon elevating the temperature, while the peak at 1385 cm<sup>-1</sup> assigned to the aliphatic C-H bending vibration of methylene groups gradually increases. Moreover, the decrease of the vibration intensities for exocyclic C=C and carboxylate groups are highly synchronized, indicating that the acrylate moieties in ZJU-199 were first decarboxylated to generate highly reactive styrene species, and subsequently thermal-polymerized to form 3D polystyrene networks under annealing conditions. UV-Vis spectra of the chloroform eluents of annealed samples showed that there is no signal ascribed to the aromatic compounds, indicating that the organic residues are highly polymerized. The organic residues suffered from severe carbonization when the temperature was raised to 500 °C and fully carbonized at 800 °C, as confirmed by Raman spectroscopy (Figure S2).

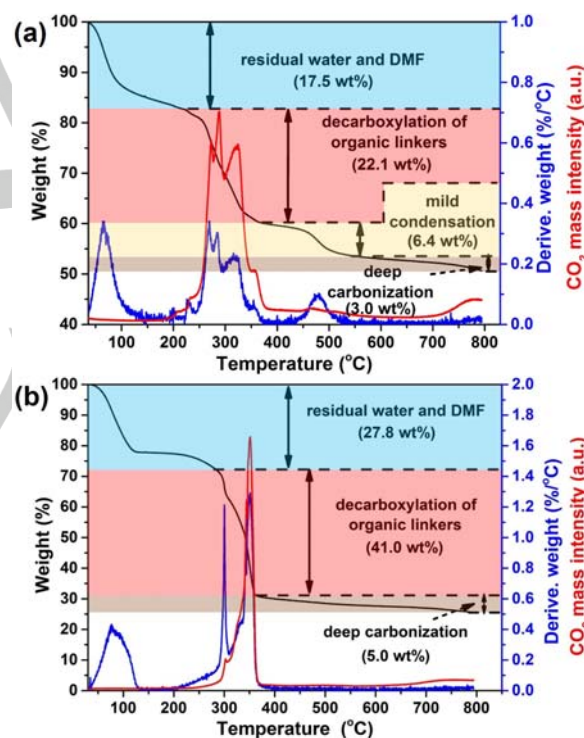
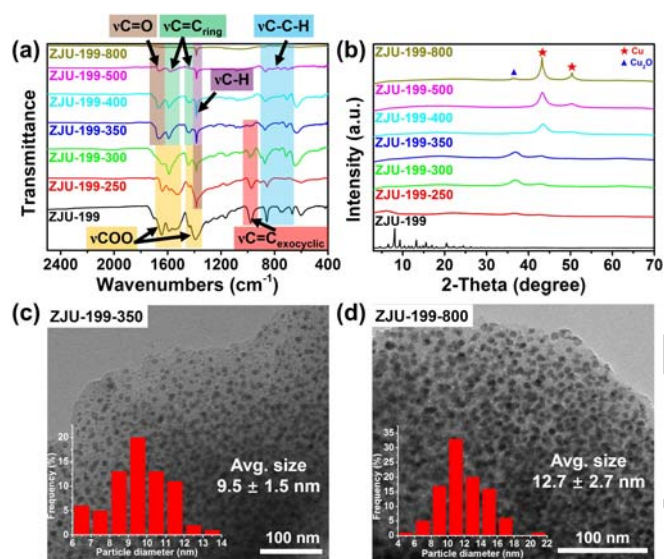


Figure 1. TG, DTG and CO<sub>2</sub>-MS curves for (a) ZJU-199 and (b) HKUST-1.

The nature of annealed samples was characterized by power X-ray diffraction (PXRD) studies (Figure 2b). Decomposition of the ZJU-199 skeleton was initiated at 250 °C, as there appeared broad and weak characteristic peaks assigned to Cu<sub>2</sub>O (JCPDS, Card No. 05-0667, 36.4°), and very weak peaks ascribed to metallic Cu (JCPDS, Card No. 04-0836, 43.2 and 50.5°). Interestingly, distinct phase transformation was observed when gradually increasing the annealing temperature. Cu<sub>2</sub>O represents the major phase in ZJU-199-300 and ZJU-199-

350 along with small amounts of metallic copper species. The  $\text{Cu}_2\text{O}$  species was gradually reduced to form  $\text{Cu}^0$  when the annealing temperature was raised to 400 °C. Deep condensation of the organic residue at higher temperature would further reduce the  $\text{Cu}_2\text{O}$  species into metallic copper species. The broad diffraction peaks of copper species in ZJU-199-T indicate that the  $\text{Cu}/\text{Cu}_2\text{O}$  particle sizes are very small, according to the Scherrer equation (Table S1). SEM images show that thermal treatment of ZJU-199 did not change the appearance of the octahedral morphology (Figure S3). TEM images show that the nanoparticles are uniformly distributed in the organic frameworks with average diameters of less than 10 nm in ZJU-199-350, which were slightly increased to 13 nm at 800 °C (Figures 2c, 2d and S4).



**Figure 2.** (a) FT-IR spectra and (b) PXRD patterns of annealed samples of ZJU-199 at different temperatures. TEM images and the corresponding histograms of metal particle size distributions for (c) ZJU-199-350 and (d) ZJU-199-800.

To understand the roles of acrylate moieties on the formation of porous organic frameworks and the in situ generation of  $\text{Cu}/\text{CuO}_x$  heterostructures, we further studied the thermal behaviors of HKUST-1, ZJU-35 and ZJU-36, consisting of zero, one and two acrylate moieties per ligand, respectively, which are isostructural to ZJU-199 (Scheme S1 and Figure S5).<sup>11b,13</sup> As shown in Figure S7, all of them are fully decarboxylated at 350 °C, and the retained organic residue mass is in the order of ZJU-199 > ZJU-36 > ZJU-35 > HKUST-1, which are proportional to the contents of acrylate groups, indicating that the acrylate groups could effectively inhibit the loss of decarboxylated organic moieties during pyrolysis. FT-IR spectrum shows that the phenyl ring vibration signals of decarboxylated organic moieties are hardly recognized for HKUST-1-300 (Figure S8). There appear the predominant peaks at 752 and 694  $\text{cm}^{-1}$  attributed to the out-of-plane bending vibration bands of substituted phenyl groups for ZJU-35-T (T =

300–400 °C), while the vibration peaks of ZJU-36-T are similar to those of ZJU-199-T. These results revealed that the acrylate moieties in organic linkers played important roles to preserve the 3D networks of the parent MOFs for the formation of organic frameworks under pyrolytic conditions. SEM images show that there are meso/macro cracks on the external surfaces of the annealed HKUST-1 samples, while the pristine morphology was almost reserved for ZJU-35 and ZJU-36 at low annealing temperature (< 400 °C) (Figures S9–S11). It is worth noting that ZJU-35-800 formed melted-like particles with round-edged octahedral morphology. This result should be ascribed to only one acrylate group per ligand in ZJU-35, which tends to form flexible 1D polystyrene chains that are easily shrunk at high temperature.<sup>14</sup> TEM images show that the diameters of NPs in different pyrolyzed samples are in the order of ZJU-199 < ZJU-36 < ZJU-35 < HKUST-1 under the same pyrolytic conditions, indicating that the acrylate moieties in Cu-MOFs could prevent the aggregation of NPs by forming physical barriers under pyrolytic conditions (Figures S12–S14).

Figure 3a shows the solid-state  $^{13}\text{C}$  magic-angle spinning (MAS) NMR spectra of copper-etched Cu-MOF-350, covering the aliphatic carbons between 0 and 80 ppm and aromatic rings from 100 to 150 ppm. The missing of the exocyclic vinyl group at ca. 110 ppm and the gradual growth of the broad  $\gamma$  peak centered at 36.5 ppm, assigned to the tertiary and secondary aliphatic carbon, further confirmed that the vinyl groups are highly polymerized.<sup>15</sup> Meanwhile, the  $\alpha$  peak intensity for HKUST-1-350 and ZJU-35-350 is relatively low, indicating that the decarboxylated benzene species is less reactive for the formation of coupled C–C bonds. The absence of the peak ascribed to the C=O moiety indicates that the decarboxylative coupling process might be the major reaction under the pyrolytic conditions.

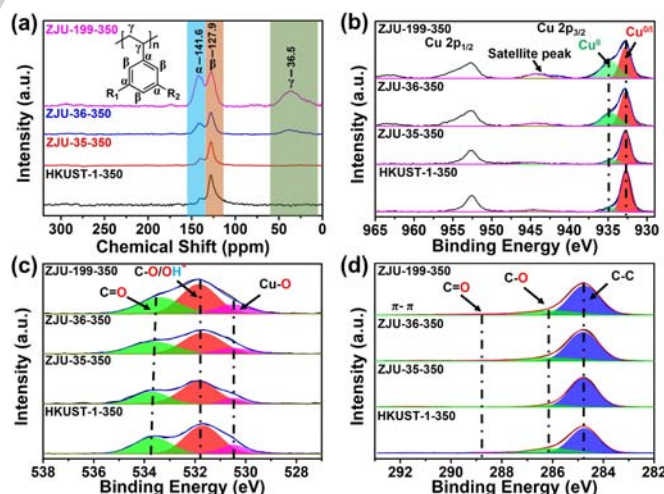


**Figure 3.** (a) Solid-state  $^{13}\text{C}$  MAS NMR spectra, and (b) Cu 2p, (c) O 1s and (d) C 1s XPS spectra of Cu-MOF-350.

To further understand the roles of acrylate groups in the pyrolytic process, we studied the thermal behaviors of MOF-143, a Cu-MOF built from  $[\text{Cu}_2(\text{COO})_4]$  SBUs and 1,3,5-benzenetribenzoate (BTB) (**Figures S16 and S17**).<sup>16</sup> FT-IR spectrum of MOF-143-350 shows that there appear an evident aromatic signal at  $1598\text{ cm}^{-1}$ , and an emerged peak at  $1734\text{ cm}^{-1}$  assigned to the ester groups, illustrating the successful reservation of the organic moieties in the pyrolyzed sample (**Figure S18**). However, there also appear the characteristic vibration bands of monosubstituted phenyl moieties at  $760$  and  $697\text{ cm}^{-1}$ , indicating insufficient cross coupling of the decarboxylated BTB moieties. This conclusion was confirmed by monitoring the UV-Vis spectrum of the chloroform eluate of MOF-143-350, which presents the absorption bands of aromatic compounds ascribed to the decarboxylated BTB monomer (1,3,5-triphenylbenzene) and coupled oligomers (**Figure S19**). PXRD profile shows that metallic copper represents the major phase in MOF-143-350 with an average diameter of  $19.5\text{ nm}$  (**Figures S20 and S21**). These characterizations revealed that pyrolysis of MOF-143 would retain most of the organic mass, attributed to the large molecule weight of BTB ligand. However, the decarboxylated BTB moieties were poorly polymerized, which could not effectively inhibit the migration of in situ generated copper species, and resulted in large aggregated NPs. These results further confirmed the important roles of acrylate groups in ZJU-199 on improving the polymerization degree, and impeding the agglomeration of in situ formed MNPs under annealing conditions.

X-ray photoelectron spectroscopy (XPS) was utilized to study the surface compositions and chemical states of the in situ formed copper species in the  $350\text{ }^\circ\text{C}$  treated samples (**Figure 3**). All samples displayed similar Cu 2p XPS spectra, where the main peaks appear in the region around  $933\text{ eV}$ , corresponding to the  $2p_{3/2}$  peaks of Cu element. Fittings of the Cu  $2p_{3/2}$  peaks resulted two components with binding energy peaks located at  $934.8$  and  $932.7\text{ eV}$  that are assigned to the surface  $\text{Cu}^{\text{II}}$  and  $\text{Cu}^{\text{I}}/\text{Cu}^0$  species, respectively.<sup>17</sup> The shake-up satellite peak at  $943\text{ eV}$  further confirmed the existence of  $\text{Cu}^{\text{II}}$  species in the pyrolyzed samples. Restricted by the low crystallinity of  $\text{Cu}^{\text{II}}$  nanospecies, no obvious diffraction peak for  $\text{CuO}$  or  $\text{Cu}(\text{OH})_2$  was found in the PXRD patterns. Because it is difficult to distinguish  $\text{Cu}^0$  and  $\text{Cu}^{\text{I}}$  from the XPS spectra, we attempted to make a distinction by Cu LMM Auger spectra. Although only a broad peak at  $916.5\text{ eV}$  for  $\text{Cu}^{\text{I}}$  species could be directly observed, we could figure out the gradual decrease of the  $\text{Cu}^0$  peak intensity at  $918.2\text{ eV}$ , accompanying increase of the acrylate contents in organic ligands (**Figure S22**). Combined with the XPS data, we calculated the  $[(\text{Cu}^0+\text{Cu}^{\text{I}})/\text{Cu}^{\text{II}}]$  atomic ratios for all samples (**Table S1**). An obvious decrease tendency of the  $[(\text{Cu}^0+\text{Cu}^{\text{I}})/\text{Cu}^{\text{II}}]$  atomic ratio was observed when increasing the acrylate contents in the pristine MOFs, which is consistent with the PXRD results.

High resolution TEM (HRTEM) images show that there are two kinds of lattice fringes with inter-planar spacing of  $0.209$  and  $0.181\text{ nm}$  assigned to the (111) and (200) of metallic Cu, respectively, where the (111) fringes of  $\text{Cu}_2\text{O}$  ( $d = 0.246\text{ nm}$ ) are located at the external surfaces of Cu NPs in HKUST-1-350 (**Figure 4a**).<sup>4d</sup> Accompanying increase of the acrylate contents in organic ligands, the ratio of metallic copper to  $\text{Cu}_2\text{O}$  in the NPs gradually decreases, which generated core-shell structures consisting of metallic Cu cores covered with thin  $\text{Cu}_2\text{O}$  layers in ZJU-35-350 and ZJU-36-350 (**Figure 4b and 4c**). As a consequence, it is difficult to discriminate the different copper species by LMM spectra.  $\text{Cu}_2\text{O}$  became the major species in the biphasic Cu/ $\text{Cu}_2\text{O}$  nanojunctions in ZJU-199-350 (**Figure 4d**). It is interesting that metallic copper is located at the edge of the multi-component heteronanostructures, resulting in highly exposed  $\text{Cu}^0$  sites and Cu/ $\text{Cu}_2\text{O}$  interfaces. Since the Cu/ $\text{Cu}_2\text{O}$  nanojunctions would generate unique local electrostatic fields at the interfaces, ZJU-199-350 might exhibit unexpected electronic properties that do not possess by discrete individuals. When the annealing temperature was increased to  $800\text{ }^\circ\text{C}$ , the copper species was highly reduced and aggregated, which resulted in heavy decrease of the accessible Cu/ $\text{Cu}_2\text{O}$  nanojunction interfaces (**Figure S24**).  $\text{N}_2$  sorption measurements revealed that ZJU-199-350 has hierarchical porous structure, which is beneficial for mass transport during catalysis (**Figures S25 and S26; Table S1**).

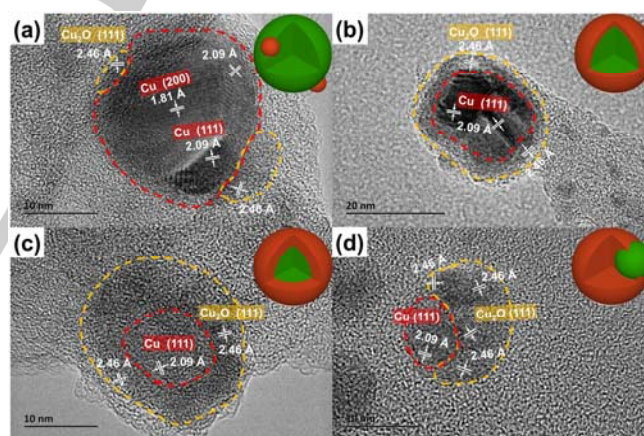


**Figure 4.** HRTEM images of (a) HKUST-1-350, (b) ZJU-35-350, (c) ZJU-36-350 and (d) ZJU-199-350 (the inserts show the schematic representations of Cu/ $\text{Cu}_2\text{O}$  heterostructures; color scheme: Cu, green;  $\text{Cu}_2\text{O}$ , red).

Biomass is an ideal class of alternatives to fossil fuels as a feedstock of fine chemicals and fuels due to its abundance and sustainability.<sup>18</sup> Furfural (FAL), as one of the major biomass platform chemicals, can be primarily produced from acid-catalyzed hydrolysis of hemicellulose and then converted into diverse chemicals and fuels.<sup>19</sup> Furfuryl alcohol (FOL), a hydrogenated product of FAL, is an important intermediate in fine chemicals and polymer industries.<sup>20</sup> The commercial production of FOL from FAL is usually performed over toxic

copper chromite under harsh conditions.<sup>21</sup> Hence, there is growing need for developing environment- and eco-friendly catalysts that could efficiently convert FAL into FOL with high activity and selectivity under mild conditions. The interesting heterostructures of Cu/Cu<sub>2</sub>O nanojunctions in the pyrolyzed Cu-MOFs prompted us to evaluate the catalytic application in hydrogenation of FAL into FOL (**Table 1**). Obviously, the pristine Cu-MOFs could not initiate the FAL hydrogenation reaction with very low yield of FOL under the catalytic conditions of 1 MPa H<sub>2</sub> and 130 °C. Meanwhile, HKUST-1 and ZJU-35 derived composites could not effectively promote the FAL hydrogenation reaction, because most of the Cu/Cu<sub>2</sub>O nanojunction interfaces in the severely aggregated copper NPs are inaccessible. As expected, great boost of the catalytic performance was achieved for ZJU-36-350 and ZJU-199-350 with 78.2 and 97.0% FOL yields, respectively. It is worth noting that ZJU-199-350 exhibits the highest turnover frequency (TOF) in the FAL hydrogenation under mild conditions, compared with the earth-abundant metal-based catalysts in the literature (**Table S2**). The high catalytic efficiency should be attributed to the small particle sizes (<10 nm) of Cu/Cu<sub>2</sub>O nanojunctions with highly exposed interfaces inside porous organic matrices.

It has been demonstrated that the electron-deficient copper species (Cu<sup>III</sup>) could perform as the Lewis acid sites to activate the carbonyl moieties by side-bond interaction.<sup>22</sup> The Cu<sup>0</sup> species is able to dissociate the absorbed H<sub>2</sub> molecules to form active hydrogen atoms, which easily react with the neighboring activated -C=O groups to produce FOL. As there are multiple nanojunction (Cu/Cu<sub>2</sub>O) interfaces on a single NP, the cooperation between Cu<sup>0</sup> and adjacent Cu<sup>III</sup> Lewis acid sites would significantly boost the catalytic performance (**Scheme S3**).<sup>23</sup> In order to confirm this assumption, the catalytic performance of FAL hydrogenation over ZJU-199-400 was also carried out, in which the Cu<sup>0</sup> was the major species with similar particle sizes in ZJU-199-350 (**Figure S27**). As expected, the FOL yield (29.3%) is dramatically decreased for ZJU-199-400, indicating the important roles of Cu<sup>III</sup> Lewis acid sites in the FAL hydrogenation reaction. Apart from the high concentration of Cu<sup>III</sup> species, the abundant accessible Cu/Cu<sub>2</sub>O heterojunction interfaces should be also accounted for the high catalytic activity of ZJU-199-350, compared with ZJU-36-350. When the annealing temperature was increased to 500 and 800 °C, only little FOL was produced for the annealed products of ZJU-36 and ZJU-199. Since negligible particle size or phase difference could be observed for the NPs in ZJU-199-400 and ZJU-199-500, the deteriorated catalytic activity should be resulted from the deep-condensation of organic moieties that could block the access of FAL molecules to the heterojunction interfaces. FT-IR spectra revealed that dehydrogenation and carbonization at 500 °C could destroy all of the functional groups in the organic supports, which resulted in weak metal-support interactions to lead to deterioration of the catalytic efficiency.

**Table 1.** Hydrogenation of FAL into FOL catalyzed by various Cu-MOFs and pyrolyzed samples.<sup>[a]</sup>

Entry	Catalyst	Conv. (%) <sup>[b]</sup>	Yield (%)	Sel. (%) <sup>[b]</sup>
1	HKUST-1	2.7	1.3	50.2
2	HKUST-1-300	3.1	2.0	66.7
3	HKUST-1-350	9.8	4.3	43.9
4	HKUST-1-400	11.4	6.2	54.1
5	HKUST-1-500	7.7	6.3	82.4
6	HKUST-1-800	5.5	3.8	68.7
7	ZJU-35	5.8	4.0	69.1
8	ZJU-35-300	19.2	4.7	24.3
9	ZJU-35-350	23.4	19.7	84.2
10	ZJU-35-400	38.5	26.4	68.7
11	ZJU-35-500	8.2	8.1	99.1
12	ZJU-35-800	9.7	4.6	47.2
13	ZJU-36	6.4	2.2	34.1
14	ZJU-36-300	74.9	70.9	94.6
15	ZJU-36-350	82.4	78.2	94.9
16	ZJU-36-400	41.1	36.3	88.3
17	ZJU-36-500	15.8	13.6	86.0
18	ZJU-36-800	8.5	2.3	27.5
19	ZJU-199	6.5	1.8	27.2
20	ZJU-199-300	71.9	70.1	97.4
21	ZJU-199-350	97.1	97.0	>99
22	ZJU-199-400	34.2	29.3	85.7
23	ZJU-199-500	7.8	4.7	60.3
24	ZJU-199-800	12.3	2.9	23.3

[a] Reaction conditions: 1.0 mmol FAL, 25 μmol catalyst (based on Cu), 2 mL isopropanol, 1 MPa H<sub>2</sub>, 130 °C, 3 h. [b] Determined by GC in the presence of *n*-octanol as the internal standard.

To comprehensively understand the reaction mechanism, a series of FAL hydrogenation experiments were conducted in the presence of ZJU-199-350 catalyst (**Figure 5**). **Figure 5a** shows the influence of reaction temperature on the catalytic performance of ZJU-199-350 in the range of 110–140 °C under 1 MPa hydrogen pressure for 3 h. The FOL yield greatly increases from 52.7% at 110 °C to 97.0% at 130 °C with retained FOL selectivity of >99%. Further elevating the reaction temperature to 140 °C did not improve the FAL conversion. The effect of reaction time on the FAL hydrogenation was also investigated (**Figure 5b**). The FOL yield increases remarkably when prolonging the reaction time from 1 to 3 h with steady FOL selectivity of >99%. The H<sub>2</sub> pressure is another important factor

that dramatically affected the catalytic results in the hydrogenation reaction. The FOL yield boosted 6-fold and 11-fold when the H<sub>2</sub> pressure was increased from 0.1 to 0.5 and 1 MPa at 130 °C for 3 h, respectively (Figure 5c). Further increase of the H<sub>2</sub> pressure could not obviously improve the catalytic results. We also tested the catalytic performance of ZJU-199-350 in various solvents, including water, toluene, methanol and isopropanol (Figure 5d). Among these solvents, water resulted in a low FOL yield of 18.6%, which should be ascribed to the reversed surface properties of hydrophilic water and hydrophobic organic matrices that could prevent the accessibility of FAL molecules to catalytic centers. The moderate FAL conversion and FOL yield in toluene should be originated from the poor H<sub>2</sub> solubility in nonpolar solvents.<sup>24</sup> For the protic organic solvents, ZJU-199-350 exhibits superior catalytic performances in isopropanol (97.0% FOL yield) and methanol (95.8% FOL yield), because hydrogen bonding between the carbonyl groups in FAL and the terminal hydroxyl groups in alcohols would help activation of the FAL molecules.<sup>22</sup>

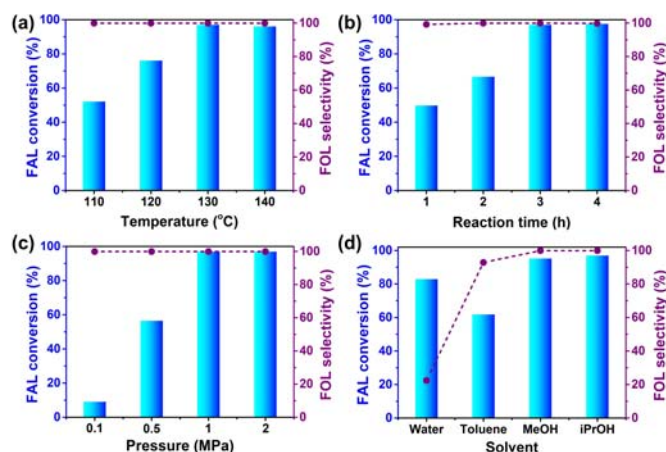


**Figure 5.** Effect of reaction conditions on hydrogenation of FAL over ZJU-199-350: (a) 1.0 mmol FAL, 25  $\mu$ mol catalyst, 2 mL isopropanol, 1 MPa H<sub>2</sub>, 3 h; (b) 1.0 mmol FAL, 25  $\mu$ mol catalyst, 2 mL isopropanol, 1 MPa H<sub>2</sub>, 130 °C; (c) 1.0 mmol FAL, 25  $\mu$ mol catalyst, 2 mL isopropanol, 130 °C, 3 h; (d) 1.0 mmol FAL, 25  $\mu$ mol catalyst, 2 mL solvent, 1 MPa H<sub>2</sub>, 130 °C, 3 h.

To obtain more insight into the hydrogenation reaction over ZJU-199-350, the kinetic behaviors were subsequently studied (Figure 6a). The reaction performed at low temperature of 100–130 °C achieved low conversions of FAL, which are beneficial for the calculations of TOF and initial reaction rates ( $r_0$ ) of the reaction. On the basis of the  $r_0$  at different temperatures, the apparent activation energy ( $E_a$ ) for ZJU-199-350 was estimated to be 57.4 kJ/mol, calculated based on the Arrhenius plot. This value is higher than the FAL adsorption energy (<30 kJ/mol), indicating that the reaction was controlled by the surface kinetics.<sup>25</sup> The high  $E_a$  value indicates that there is strong interaction between FAL molecules and copper sites, which could assist the adsorption and activation of FAL to promote the hydrogenation reaction. Meanwhile, the strong FAL adsorption over copper catalysts could be greatly diminished by raising the

reaction temperature, and thus to greatly increase the reaction rate.

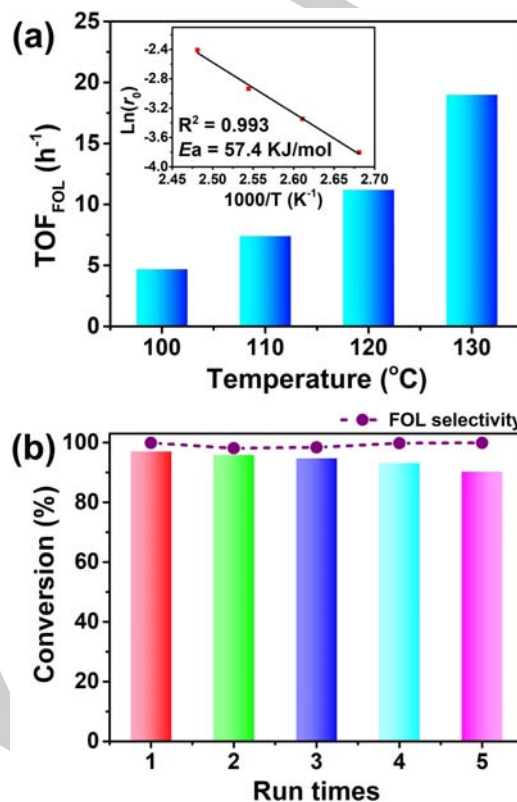


**Figure 6.** Kinetic studies of FAL hydrogenation over ZJU-199-350 catalyst: (a) reaction rates of ZJU-199-350 at different temperatures (the inset represents the Arrhenius plot for the FAL hydrogenation). Reaction conditions: 2.5 mmol FAL, 5 mL isopropanol, 25  $\mu$ mol catalyst, 1 MPa H<sub>2</sub>, 100–130 °C, 2 h. (b) The recyclability of ZJU-199-350 for the hydrogenation of FAL. Reaction conditions: 1.0 mmol FAL, 25  $\mu$ mol catalyst, 2 mL isopropanol, 1 MPa H<sub>2</sub>, 130 °C, 3 h.

We further evaluated the stability and recyclability of ZJU-199-350 for the FAL hydrogenation reaction. The catalyst showed stable activity and selectivity for five successive runs in the FAL hydrogenation (Figure 6b). FT-IR spectrum of the spent catalyst demonstrated that the organic framework was well preserved after catalysis, and no obvious metal leaching was found as revealed by ICP-OES (Figure S28 and Table S3). Compared with the fresh ZJU-199-350, the spent catalyst exhibits similar XRD profile (Figure S29). XPS results showed that the Cu<sup>II</sup> content slightly decreased after catalysis, indicating that partial Cu<sup>III</sup> species was reduced during the hydrogenation reaction (Figure S30). It is worth noting that no obvious particle agglomeration, phase separation or core-shell Cu/Cu<sub>2</sub>O heterojunction formation was observed in the spent ZJU-199-350, indicating the important roles of the organic framework matrices on stabilizing the Cu/Cu<sub>2</sub>O heterostructures by serving as the physical barriers (Figure S31).

## Conclusion

In summary, we successfully regulated the particle sizes, phase compositions and nanostructures of the encapsulated Cu/Cu<sub>2</sub>O nanojunctions in organic frameworks derived from Cu-MOFs by tuning the ligand structures and pyrolytic conditions. Promotion of the polymerization degree of decarboxylated organic moieties was achieved by introducing exocyclic acrylate groups in organic linkers of Cu-MOFs. The highly polymerized porous organic matrices could efficiently prevent the agglomeration of in situ generated NPs under annealing conditions, which formed stable Cu/Cu<sub>2</sub>O nanojunctions with abundant accessible interfaces inside porous organic matrices. The facily prepared Cu/Cu<sub>2</sub>O@organic framework composite material ZJU-199-350 exhibits superior catalytic activity, selectivity and stability in hydrogenation of FAL into FOL. This work provides a unique perspective for the generation of accessible metal/metal oxide nanojunctions inside organic frameworks derived from MOFs for highly efficient heterogeneous catalysis.

## Acknowledgements

We are grateful for the financial support of the National Natural Science Foundation of China (grant nos. 21525312 and 21872122).

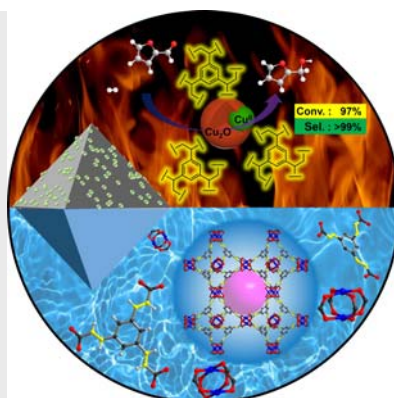
**Keywords:** Metal-organic frameworks • Organic framework materials • Composite materials • Heterojunctions • Catalysis

- [1] (a) H.-L. Liu, F. Nosheen, X. Wang, *Chem. Soc. Rev.* **2015**, *44*, 3056-3078; (b) J. Wang, G. Dong, *Chem. Rev.* **2019**, *119*, 7478-7528; (c) D. Pflästerer, A. S. K. Hashmi, *Chem. Soc. Rev.* **2016**, *45*, 1331-1367.
- [2] (a) D. Wang, D. Astruc, *Chem. Soc. Rev.* **2017**, *46*, 816-854; (b) P. Gandeepan, T. Müller, D. Zell, G. Cera, S. Warratz, L. Ackermann, *Chem. Rev.* **2019**, *119*, 2192-2452.
- [3] (a) C. Ray, T. Pal, *J. Mater. Chem. A* **2017**, *5*, 9465-9487; (b) B. Zhang, J. Liu, J. Wang, Y. Ruan, X. Ji, K. Xu, C. Chen, H. Wan, L. Miao, J. Jiang, *Nano Energy* **2017**, *37*, 74-80; (c) H. Robatjazi, H. Zhao, D. F. Swearer, N. J. Hogan, L. Zhou, A. Alabastri, M. J. McClain, P. Nordlander, N. J. Halas, *Nat. Commun.* **2017**, *8*, 27; (d) R. Boppella, C. H. Choi, J. Moon, D. H. Kim, *Appl. Catal. B: Environ.* **2018**, *239*, 178-186.
- [4] (a) M. B. Gawande, A. Goswami, F.-X. Felpin, T. Asefa, X. Huang, R. Silva, X. Zou, R. Zboril, R. S. Varma, *Chem. Rev.* **2016**, *116*, 3722-3811; (b) N. K. Ojha, G. V. Zyryanov, A. Majee, V. N. Charushin, O. N. Chupakhin, S. Santra, *Coord. Chem. Rev.* **2017**, *353*, 1-57; (c) S. Zhang, Y. Ma, H. Zhang, X. Zhou, X. Chen, Y. Qu, *Angew. Chem. Int. Ed.* **2017**, *56*, 8245-8249; (d) X. Chang, T. Wang, Z.-J. Zhao, P. Yang, J. Greeley, R. Mu, G. Zhang, Z. Gong, Z. Luo, J. Chen, Y. Cui, G. A. Ozin, J. Gong, *Angew. Chem. Int. Ed.* **2018**, *57*, 15415-15419; (e) P. Ling, Q. Zhang, T. Cao, F. Gao, *Angew. Chem. Int. Ed.* **2018**, *57*, 6819-6824; (f) S.-C. Qi, X.-Y. Qian, Q.-X. He, K.-J. Miao, Y. Jiang, P. Tan, X.-Q. Liu, L.-B. Sun, *Angew. Chem. Int. Ed.* **2019**, *58*, 10104-10109; (g) R. T. Yang, A. J. Hernández-Maldonado, F. H. Yang, *Science* **2003**, *301*, 79-81.
- [5] (a) R. Zhang, L. Hu, S. Bao, R. Li, L. Gao, R. Li, Q. Chen, *J. Mater. Chem. A* **2016**, *4*, 8412-8420; (b) H. Xu, J.-X. Feng, Y.-X. Tong, G.-R. Li, *ACS Catal.* **2017**, *7*, 986-991; (c) Y. Song, H. Wang, G. Liu, H. Wang, L. Li, Y. Yu, L. Wu, *J. Catal.* **2019**, *370*, 461-469.
- [6] J. Song, J. Li, J. Xu, H. Zeng, *Nano Lett.* **2014**, *14*, 6298-6305.
- [7] (a) X. Jing, C. He, L. Zhao, C. Duan, *Acc. Chem. Res.* **2019**, *52*, 100-109; (b) K. Lu, T. Aung, N. Guo, R. Weichselbaum, W. Lin, *Adv. Mater.* **2018**, *30*, 1707634; (c) G. Maurin, C. Serre, A. Cooper, G. Férey, *Chem. Soc. Rev.* **2017**, *46*, 3104-3107; (d) H. Wang, X. Dong, V. Colombo, Q. Wang, Y. Liu, W. Liu, X.-L. Wang, X.-Y. Huang, D. M. Proserpio, A. Sironi, Y. Han, J. Li, *Adv. Mater.* **2018**, *30*, 1805088; (e) B. Liu, H. Shioyama, T. Akita, Q. Xu, *J. Am. Chem. Soc.* **2008**, *130*, 5390-5391; (f) L. Jiao, Y. Wang, H.-L. Jiang, Q. Xu, *Adv. Mater.* **2018**, *30*, 1703663; (g) S. J. Yang, S. Nam, T. Kim, J. H. Im, H. Jung, J. H. Kang, S. Wi, B. Park, C. R. Park, *J. Am. Chem. Soc.* **2013**, *135*, 7394-7397; (h) Z. Bao, G. Chang, H. Xing, R. Krishna, Q. Ren, B. Chen, *Energy Environ. Sci.* **2016**, *9*, 3612-3641; (i) B. Y. Guan, X. Y. Yu, H. B. Wu, X. W. Lou, *Adv. Mater.* **2017**, *29*, 1703614; (j) Y.-Z. Chen, R. Zhang, L. Jiao, H.-L. Jiang, *Coord. Chem. Rev.* **2018**, *362*, 1-23; (k) Q.-G. Zhai, X. Bu, X. Zhao, D.-S. Li, P. Feng, *Acc. Chem. Res.* **2017**, *50*, 407-417; (l) X. Lian, Y. Fang, E. Joseph, Q. Wang, J. Li, S. Banerjee, C. Lollar, X. Wang, H.-C. Zhou, *Chem. Soc. Rev.* **2017**, *46*, 3386-3401.
- [8] (a) W. Bak, H. S. Kim, H. Chun, W. C. Yoo, *Chem. Commun.* **2015**, *51*, 7238-7241; (b) K. Zhao, Y. Liu, X. Quan, S. Chen, H. Yu, *ACS Appl. Mater. Interfaces* **2017**, *9*, 5302-5311; (c) X. Liu, D. Xu, L. Zhang, *ACS Sustainable Chem. Eng.* **2017**, *5*, 7800-7811; (d) Y. Wang, Y. Lü, W. Zhan, Z. Xie, Q. Kuang, L. Zheng, *J. Mater. Chem. A* **2015**, *3*, 12796-12803; (e) H. Niu, S. Liu, Y. Cai, F. Wu, X. Zhao, *Microporous Mesoporous Mater.* **2016**, *219*, 48-53; (f) A. K. Kar, R. Srivastava, *Inorg. Chem. Front.* **2019**, *6*, 576-589; (g) K. Yang, Y. Yan, H. Wang, Z. Sun, W. Chen, H. Kang, Y. Han, W. Zhang, X. Sun, Z. Li, *Nanoscale* **2018**, *10*, 17647-17655.
- [9] E. Scott, F. Peter, J. Sanders, *Appl. Microbiol. Biotechnol.* **2007**, *75*, 751-762.
- [10] K. Chen, C.-D. Wu, *Angew. Chem. Int. Ed.* **2019**, *58*, 8119-8123.
- [11] (a) L. Zhang, C. Zou, M. Zhao, K. Jiang, R. Lin, Y. He, C.-D. Wu, Y. Cui, B. Chen, G. Qian, *Cryst. Growth Des.* **2016**, *16*, 7194-7197; (b) S. S.-Y. Chui, S. M.-F. Lo, J. P. H. Charmant, A. G. Orpen, I. D. Williams, *Science* **1999**, *283*, 1148-1150.
- [12] (a) R. Dabestani, P. F. Britt, A. C. Buchanan, *Energy Fuels* **2005**, *19*, 365-373; (b) N. M. Sánchez, A. de Klerk, *Thermochim. Acta* **2018**, *662*, 23-40.
- [13] G.-Q. Kong, Z.-D. Han, Y. He, S. Ou, W. Zhou, T. Yildirim, R. Krishna, C. Zou, B. Chen, C.-D. Wu, *Chem. Eur. J.* **2013**, *19*, 14886-14894.
- [14] H. Gu, C. Ma, C. Liang, X. Meng, J. Gu, Z. Guo, *J. Mater. Chem. C* **2017**, *5*, 4275-4285.
- [15] (a) R. V. Law, D. C. Sherrington, C. E. Snape, *Macromolecules* **1996**, *29*, 6284-6293; (b) I. van Zandvoort, E. J. Koers, M. Weingarh, P. C. A. Bruijninx, M. Baldus, B. M. Weckhuysen, *Green Chem.* **2015**, *17*, 4383-4392.
- [16] H. Furukawa, Y. B. Go, N. Ko, Y. K. Park, F. J. Uribe-Romo, J. Kim, M. O'Keeffe, O. M. Yaghi, *Inorg. Chem.* **2011**, *50*, 9147-9152.
- [17] J. P. Espinós, J. Morales, A. Barranco, A. Caballero, J. P. Holgado, A. R. González-Elipe, *J. Phys. Chem. B* **2002**, *106*, 6921-6929.
- [18] H. Wang, J. Male, Y. Wang, *ACS Catal.* **2013**, *3*, 1047-1070.
- [19] (a) L. T. Mika, E. Cséfalvay, Á. Németh, *Chem. Rev.* **2018**, *118*, 505-613; (b) W. Leitner, J. Klankermayer, S. Pischinger, H. Pitsch, K. Kohse-Höinghaus, *Angew. Chem. Int. Ed.* **2017**, *56*, 5412-5452.
- [20] K. Yan, G. Wu, T. Lafleur, C. Jarvis, *Renew. Sustain. Energy Rev.* **2014**, *38*, 663-676.
- [21] B. M. Nagaraja, V. S. Kumar, V. Shasikala, A. H. Padmasri, B. Sreedhar, B. D. Raju, K. S. R. Rao, *Catal. Commun.* **2003**, *4*, 287-293.
- [22] W. Gong, C. Chen, Y. Zhang, H. Zhou, H. Wang, H. Zhang, Y. Zhang, G. Wang, H. Zhao, *ACS Sustainable Chem. Eng.* **2017**, *5*, 2172-2180.
- [23] G.-P. Zhan, C.-D. Wu, *Sci. Bull.* **2019**, *64*, 385-390.
- [24] M. J. Taylor, L. J. Durndell, M. A. Isaacs, C. M. A. Parlett, K. Wilson, A. F. Lee, G. Kyriakou, *Appl. Catal. B: Environ.* **2016**, *180*, 580-585.
- [25] S. Sitthitha, T. Sooknoi, Y. Ma, P. B. Balbuena, D. E. Resasco, *J. Catal.* **2011**, *277*, 1-13.

## Entry for the Table of Contents

## RESEARCH ARTICLE

A strategy to generate and stabilize Cu/Cu<sub>2</sub>O nanojunctions inside porous organic frameworks is developed by controlled pyrolysis of metal-organic frameworks, which results in a composite material that consists of easily accessed Cu/Cu<sub>2</sub>O heterojunctions inside porous organic matrices, exhibiting excellent catalytic properties in hydrogenation of furfural into furfuryl alcohol.



Kai Chen, Jia-Long Ling and Chuan-De Wu\*

Page No. – Page No.

**In situ Generation and Stabilization of Accessible Cu/Cu<sub>2</sub>O Heterojunctions inside Organic Frameworks for Highly Efficient Catalysis**

Accepted Manuscript